Airborne Differential SAR Interferometry: First Results at L-Band

Andreas Reigber, *Member, IEEE*, and Rolf Scheiber

***Abstract*—In recent years, differential interferometry using spaceborne synthetic aperture radar (SAR) sensors has become an established technique for detecting and monitoring centimeter-scale deformations of the earth's surface, as well as glacier flows and land slides. Although often very efficient, the use of spaceborne SAR data has several drawbacks, namely phase artifacts caused by atmospheric effects and very low coherence due to long data acquisition intervals and the short radar wavelength of the sensor. Most important, current spaceborne sensors are not able to ensure flexible monitoring of critical regions. Airborne sensors may overcome most of the problems mentioned above, but up to now, the operational use of airborne differential SAR interferometry has been prevented by insufficiently accurate motion compensation of the platform. In this letter, first results of airborne differential interferometry using the German Aerospace Center (DLR) experimental SAR system (E-SAR) in the interferometric repeat-pass mode are addressed. This includes an analysis of long-term decorrelation behavior in L-band and, particularly, the correction of residual motion errors in heavily decorrelated interferograms. A first differential interferogram of agricultural and forested areas is presented and analyzed.**

***Index Terms*—Airborne, differential interferometry, motion errors, synthetic aperture radar (SAR).**

I. Introduction

THE PRINCIPAL idea of differential synthetic aperture radar (SAR) interferometry is to analyze phase effects in SAR interferograms, which are not related to the terrain topography [1]. In general, the interferometric phase difference between two SAR images taken at different times and from slightly different positions can be expressed as

$$\Phi = \Phi_{\mathrm{topo}} + \Phi_{\mathrm{fe}} + \Phi_n + \Phi_{\mathrm{atm}} + \Phi_{\Delta r} \tag{1}$$

with Φ_{topo} denoting the phase contribution caused by terrain topography, Φ_{fe} the systematic phase component corresponding to flat earth, Φ_n a noise contribution due to limited SNR and temporal decorrelation effects, Φ_{atm} a phase contribution due to different atmospheric conditions for two datasets, and $\Phi_{\Delta r}$ the differential phase related to changes in the slant-range distance.

In differential interferometry, $\Phi_{\Delta r}$ is estimated by subtracting Φ_{topo} and Φ_{fe}, either by using an external digital elevation model (DEM) or a second interferogram without differential effects. The effects of atmosphere may be eliminated by investigation of long time series [2]–[4] or by modeling tropospheric delays through simultaneous evaluation of global positioning system measurements [5].

This letter addresses the use of airborne SAR sensors for differential interferometry. On one hand, the availability of long wavelengths with better coherence behavior, like L- or P-band, offers the possibility of an analysis of long-term processes even in case of vegetated areas. Also, on the other hand, the capabilities for monitoring short-term processes are improved by the greater flexibility of airborne sensors.

The main problem of processing airborne SAR data is the compensation of the aircraft movement. In this case, the term $\Phi_{\Delta r}$ consists of two contributions, one caused by displacements of the scattering center and one caused by displacements of the sensor platform. Hence, determination of the surface displacement requires an accurate estimation and correction of the sensor motion. For example, an uncompensated sensor motion of only half the wavelength (12 cm in L-band) causes a phase error of 360°. Thus, even in L-band, it is indispensable to reach millimeter precision in SAR motion compensation in order to allow the data to be used for differential interferometry applications.

The principal feasibility of airborne differential interferometry has already been demonstrated in [6], where the movements of a reflector have been extracted from their phase shifts relative to the background phase. In this letter, first steps toward a fully two-dimensional measurement of the phase displacement field, using airborne differential SAR interferometry, are illustrated. This includes an analysis of the coherence of L-band SAR images of vegetated areas with very long temporal baselines. Preliminary results, using L-band data acquired by the experimental SAR (E-SAR) sensor of the German Aerospace Center (DLR) [7], are shown.

II. Motion Compensation

As mentioned before, the generation of interferograms using airborne sensors requires an accurate compensation of the deviations of the aircraft from the ideal straight flight track. It has been proven that motion errors of up to some tens of meters can be easily compensated by advanced processing algorithms if the errors are precisely measured [8]. However, current navigation systems provide only a position accuracy of about 5–10 cm. Therefore, in L-band, phase errors of up to 2π can be expected.

In order to correct for these residual phase errors, the interferogram phase correction proposed in [9] has been applied. It is based on the fact that residual motion errors are causing azimuth displacements in the image, which are measured during the coregistration of the interferometric image pair. Assuming that the motion error has locally a linear characteristic, i.e., if

Manuscript received December 3, 2002; revised April 23, 2003.

A. Reigber is with the Department of Photogrammetry and Cartography, Technical University of Berlin, Berlin 10623, Germany.

R. Scheiber is with the Microwaves and Radar Institute, German Aerospace Center (DLR), Oberpfaffenhofen 82230, Germany.

Digital Object Identifier 10.1109/TGRS.2003.814610

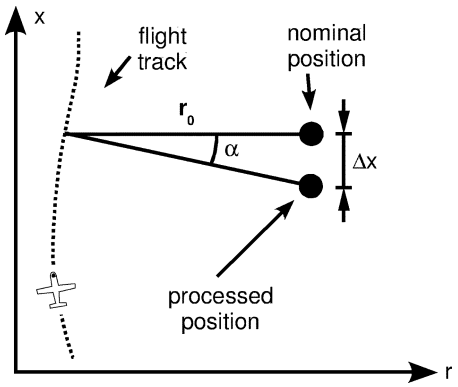

Fig. 1. Azimuth displacement caused by inaccurate motion compensation.

the real track is rotated by an angle $\alpha(x)$ with respect to the measured one, the zero-Doppler position of a target, located in range at distance r_0 and at azimuth position x, becomes shifted by (compare Fig. 1)

$$\Delta x(x) = -r_0 \sin \alpha(x). \tag{2}$$

Processing such data, the peak of the impulse response will appear shifted in azimuth by this amount. Measuring the coregistration function in azimuth $\Delta x(x)$, the total residual motion error in the interferogram $\Delta r(x)$ can be estimated by integrating the rotation angle α over azimuth

$$\Delta r(x) = \int_0^x \frac{\Delta x(x')}{r_0}\,\mathrm{d}x' + C. \tag{3}$$

Except for an integration constant C, which corresponds to a global baseline offset, this function can be obtained from the data itself. The unknown baseline offset has been set to zero here, introducing possibly a phase error along range. From the observed variations of Δr along azimuth, a baseline error of about 5–10 cm can be expected. It is possible to estimate this unknown baseline offset using ground control points, if available, or an external DEM as suggested in [15]. However, in this study, this has not been done, as the current capabilities of the experimental setup alone should be demonstrated.

The limitation of this method is the precision of the used coregistration method and its spatial resolution. As a first step, conventional coregistration based on speckle correlation and coherence optimization has been applied. Twenty patches over range and 40 patches over azimuth, each sized 256×256 pixels, have been used for the image size of 2048 pixels in range by 4096 pixels in azimuth. A three-step reliability check of the measured parameters has been implemented to avoid errors in low-coherent areas. Patches exceeding a maximum offset value of four pixels and those without a distinct peak in their cross-correlation function are discarded. Additionally, it is checked that different patch sizes give the same result. The canceled offsets were finally interpolated from the known ones using thin plate splines. After this first-order coregistration, the spectral diversity method [10] has been applied to allow highly accurate coregistration estimates combined with high spatial resolution. The resulting total coregistration errors were found to have a variance of about 10 cm, with typical wavelengths in its variations along azimuth of 200–300 m. Due to the low coherence of some interferograms, coherence weighting and strong averaging of the obtained coregistration function along the range dimension were necessary to avoid propagation errors during the subsequent integration step.

III. Long-Term Coherence Analysis

In order to get an impression of the degree of coherence that can be expected from airborne L-band data, the baselines of all calibration flights performed in L-band over the Oberpfaffenhofen test site during the last two years have been investigated. While the critical baseline is about 200 m for E-SAR in L-band, several data pairs with mean horizontal baselines below 10 m were acquired. However, random vertical baselines up to 300 m have been encountered, due to the usual dependence of the flight level on barometric altitude. This has restricted the useful number of scenes to a total number of four. It has to be noted that in dedicated interferometric missions the E-SAR carrier, a Do-228, is capable of navigating with a precision of about 5–10 m [7], allowing each track to be suitable for repeat-pass interferometry.

The useful tracks have been acquired on June 15, 2000 (track 1), September 15, 2000 (track 2), and August 27, 2001 (tracks 3 and 4, 12 min temporal baseline), all with mean perpendicular baselines between the tracks below 10 m. The resulting coherence maps in horizontal–horizontal (HH) and vertical–vertical (VV) polarization are shown in Fig. 2. During data processing, all four datasets have been coregistered precisely to the geometry of track 3. Due to the short baselines involved, it was not necessary to filter spectral decorrelation effects in range. The real Doppler centroid of the datasets was found to be in between -30 and 30 Hz. However, due to the relative wide beamwidth of the E-SAR antenna, azimuth processing could be performed to a common Doppler bandwidth of 100 Hz centered at 0 Hz.

Large areas of the Oberpfaffenhofen airfield remain correlated even after almost one year. This behavior is observed not only for the runway, but also for the surrounding meadows. The L-band response is not influenced too strongly by the reflection from the vegetation; instead it seems to possess a stable contribution originating from the soil below. This assumption is supported by the observation that the coherence γ does not decrease significantly from the three-month to the one-year time interval. The coherence of the meadow is higher in VV ($\gamma_{\mathrm{vv}} \approx 0.7$) than in HH ($\gamma_{\mathrm{hh}} \approx 0.5$), which is supposedly due to the stronger surface reflection in VV, leading to a better SNR compared to HH.

The agricultural fields show different behavior. Some of them stay correlated, while others loose their coherence. This is expected, as fields that are ploughed between data acquisitions should decorrelate completely. Again a higher coherence can be observed in VV polarization than in HH polarization. The coherence of some untouched fields even increases after one year compared to the three-month coherence (from $\gamma_{\mathrm{vv}} = 0.4$ to $\gamma_{\mathrm{vv}} = 0.6$). This is probably due to the different season for the three-month temporal baseline, while the season is almost the same for tracks 2 and 3.

Even after almost one year, the forested areas do not appear completely decorrelated, both in HH ($\gamma_{\mathrm{hh}} \approx 0.3$ to 0.4) and VV polarization ($\gamma_{\mathrm{vv}} \approx 0.2$ to 0.3). It can be assumed that the

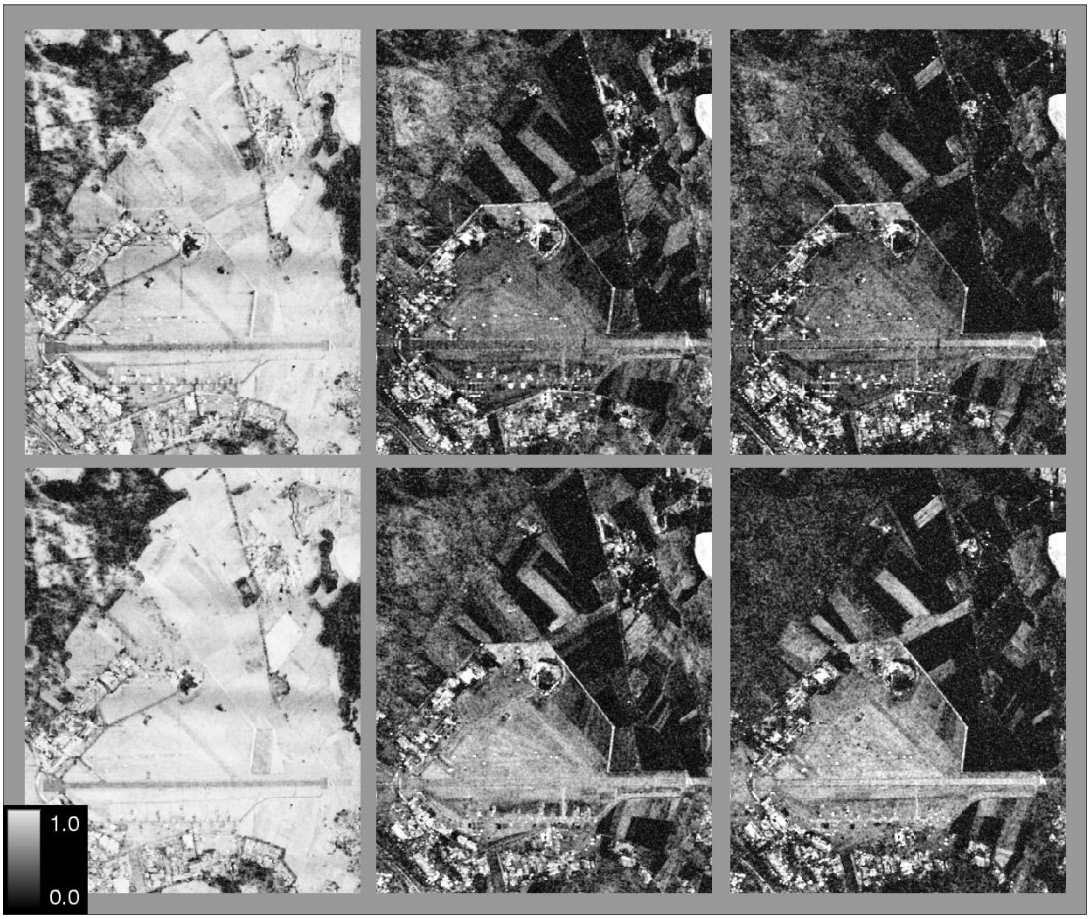

Fig. 2. Slant-range coherence maps of the Oberpfaffenhofen test site (latitude 48.085N°, longitude: 11.292E°) in (top) HH) and (bottom) VV polarization. The temporal baseline varies from 12 min on the left side (tracks 3 and 4) over 92 days in the middle (tracks 1 and 2) to 336 days on the right side (tracks 2 and 3). Nominal horizontal baselines are 10 m (tracks 3 and 4) and 0 m (tracks 1 and 2 and tracks 2 and 3). Azimuth direction: Right side, from bottom to top, left looking.

double-bounce echo, i.e., the ground–stem interaction generates a quite stable contribution to the measured signals. A strong indication for this is that the long-term coherence of forest is better in HH than in VV polarization, as a double-bounce contribution appears stronger in the HH than in the VV channel [11].

IV. Generation of Differential Interferograms

For the generation of a differential interferogram, the short-term interferogram between tracks 3 and 4 has been used for estimating the topography. Apart from its high coherence, it has a significant baseline of about 10 m, corresponding to a 2π ambiguity of about 20 m in midrange. For the long-term interferogram, tracks 2 and 3 were chosen, because after one year at least some differential effects can be expected. The baseline between these two tracks is very small, between 1 and 5 m, depending on the azimuth position. The actual differential interferogram is calculated using a simple approach: using the factor between the two baseline values, the unwrapped and flattened interferometric phase [12] between tracks 3 and 4 Φ_{34} can be scaled to the geometry of tracks 3 and 2 [13]. In this way, the topographic effects in the long-term interferogram are eliminated

$$\Phi_{\Delta r} = \Phi_{32} - \frac{B_{32}}{B_{34}}\Phi_{34} \tag{4}$$

with B_{32} and B_{34} denoting the normal baseline component between tracks 3 and 2, respectively tracks 3 and 4, and Φ_{32} and Φ_{34} the two unwrapped interferometric phases after flat-earth phase removal and correction of the phase offset introduced by the phase-unwrapping procedure. It has to be noted that in the airborne case the normal baseline components are varying strongly with both range distance (incidence angle variation) and azimuth position (nonlinear flight tracks). During flat-earth phase removal and phase scaling, this has to be taken into account precisely. However, even after flat-earth removal, both interferograms involved show some residual flat-earth-phase-like phase components, which are related to residual motion errors in the data.

Consequently, also the resulting differential interferogram contains some unwanted flat-earth phase-like phase component, both in range and azimuth. The range component might be due to a constant baseline error, while the almost linear azimuth component might result from a small systematic error in the estimation of $\Delta x(x')$ [see (3)]. To compensate these effects, a linear phase component in azimuth and a $1/\sin\theta$ phase component in range has been fitted to the data, with θ denoting the off-nadir angle. In the following, these components, as well as the mean phase of the resulting differential interferogram, have been subtracted from the data.

The final differential interferogram is shown in Fig. 3. One phase cycle corresponds to a displacement in line-of-sight direc-

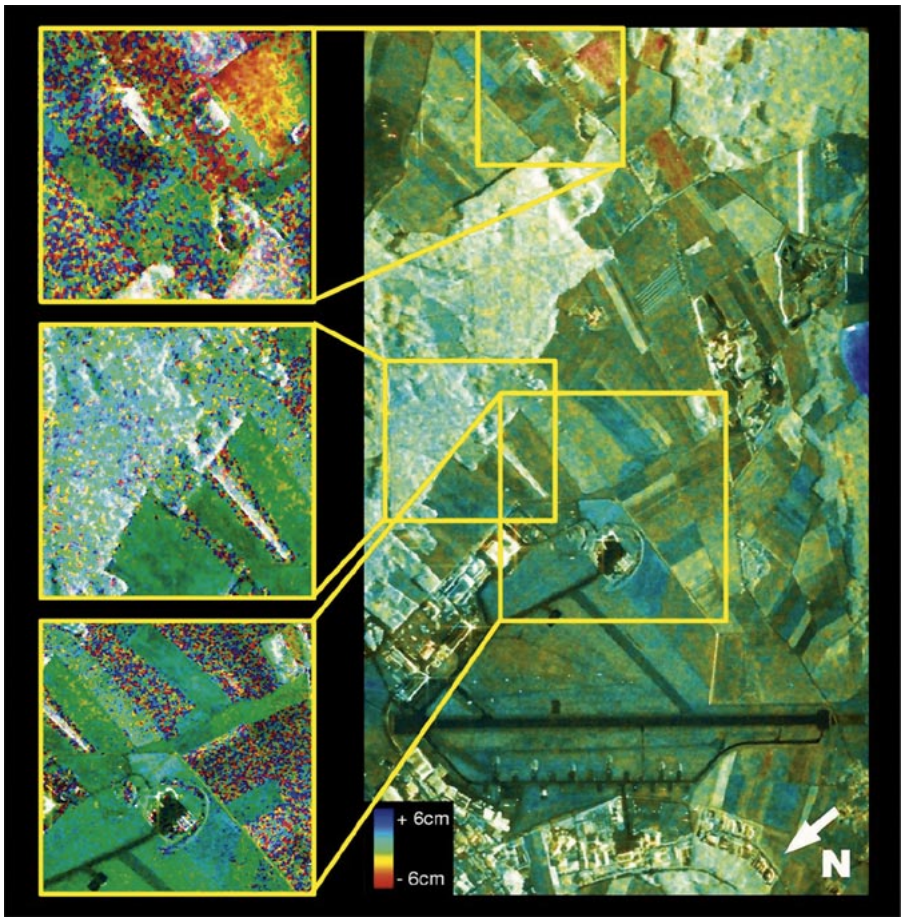

Fig. 3. Overlay of SAR amplitude (magnitude) and differential interferogram (color) of the Oberpfaffenhofen test site, using track 2 (September 15, 2000) and track 3 (August 27, 2001). The scene extension is 2.5 km in range × 5 km in azimuth. The differential phase corresponds to displacements in line-of-sight direction from (red) −6 cm to (blue) +6 cm. (Left) Magnification of three areas of interest. (Right) Azimuth direction:, from bottom to top, left looking.

tion of 12 cm. The Oberpfaffenhofen test site is an area where generally no surface displacements are expected. Therefore, the final differential interferogram reflects mainly the quality of the data processing. Any uncompensated motion error should be visible as phase variations along azimuth. It can be observed that this is not the case, except the flat-earth-like terms mentioned before, which have been removed.

Despite these uncertainties, the generated phase displacement map shows several interesting effects, which are related to individual features in the image. In the large coherent area of the airfield, a significant phase displacement does not take place. But on some of the agricultural fields, present around the airport, phase displacements can be observed. Depending on the respective field, both positive and negative movement directions occur. The edges in the displacement map correlate well with field boundaries in the SAR amplitude image. It is unlikely that the observed phase displacements are related to changes in vegetation height. The backscattering component of vegetation, particularly after one year and with different heights, should not be coherent. Possible explanations are local changes in the soil moisture, causing different penetration depths. Similar effects have also been noted by Gabriel *et al.* using L-band spaceborne data of the Seasat satellite [1].

The same question arises for the forested areas in the upper right and in the middle of the image. In both areas, the dark coloring in Fig. 3 indicates a slight rise of the location of the backscattering. Whether these are processing artifacts or have some physical explanation has to be clarified by further investigations.

The area appearing in blue in the near range of the image is a swamp area. It shows up with constant high coherence over long periods of time due to the dominant contribution of the double-bounce scattering from the water area and the plants stipes. We attribute the rise of 5 cm of the backscatter center to a change in the surface water level in this area. Similar effects have been reported by Alsdorf *et al.* [14] using SIR-C data.

V. Discussion and Conclusion

The airborne repeat-pass data processing for differential interferometry is challenging and not yet completely stable. More work is necessary in this area. Up to now, good differential interferograms cannot be generated from every dataset. The quality of the acquired motion data still seems to have a crucial influence on the final image phase, although residual errors should, in principle, get compensated automatically. Also, for the moment, residual flat-earth-like components in both range and azimuth are unavoidable.

One problem of the residual motion error correction is that it is based on integration. It cannot be used, therefore, to solve for a constant baseline offset without using ground control points. This, as well as problems with the overall calibration

of the sensor geometry, might be the reason for the observed flat-earth-like phase in range. Additionally, a small constant offset in the azimuthal coregistration would cause a linear error of the correction phase in azimuth, which could explain the observed linear effect in azimuth. Further investigations are necessary to find a more stable way for the correction of residual motion errors. Some ideas have already been presented in [15].

The preliminary results of airborne differential interferometry, as presented in Fig. 3, show several interesting effects, particularly happening on vegetated areas. Most of the observed changes in the scattering center heights are supposedly not related to surface deformations, but to soil moisture changes. As there are no ground measurements available, this assumption cannot be checked for the currently available datasets. A mission dedicated specially to differential interferometry is indispensable to clarify this point. However, the basic feasibility of airborne differential SAR interferometry was clearly shown by the presented results.

Additionally, it has been demonstrated in this letter that the SAR backscattering in L-band is stable enough to provide acceptable coherence over vegetated areas, even after one year. L-band seems to be a well-suited wavelength for long-term differential interferometry. Particularly, the combination of operationally generated spaceborne interferometric L-band SAR data (e.g., the Advanced Land Observing Satellite [16]) with flexibly acquired airborne data seems to be very promising in future.

ACKNOWLEDGMENT

The authors appreciate the valuable comments and suggestions of the anonymous reviewers. They helped the understanding of the observed features and thus improved the contents of this letter.

REFERENCES

[1] A. Gabriel, R. M. Goldstein, and H. A. Zebker, "Mapping small elevation changes over large areas: Differential radar interferometry," *J. Geophys. Res.*, vol. 94, no. B7, pp. 9183–9191, 1989.

[2] A. Ferretti, C. Prati, and F. Rocca, "Nonlinear subsidence rate estimation using permanent scatterers in differential SAR interferometry," *IEEE Trans. Geosci. Remote Sensing*, vol. 38, pp. 2202–2212, Sept. 2000.

[3] D. Massonet, M. Rossi, C. Carmona, F. Adragna, G. Pelzer, K. Feigl, and T. Rabaute, "The displacement field of the landers earthquake mapped by radar interferometry," *Nature*, vol. 364, pp. 138–142, 1993.

[4] R. Kwock and M. A. Fahnestock, "Ice sheet motion and topography from radar interferometry," *IEEE Trans. Geosci. Remote Sensing*, vol. 34, pp. 189–220, Jan. 1996.

[5] P. W. Webley, R. M. Bingley, A. H. Dodson, G. Wadge, S. J. Waugh, and I. N. James, "Atmospheric water vapor correction to InSAR surface motion measurement on mountains: Results from a dense GPS network on mount etna," *Phys. Chem. Earth*, vol. 27, pp. 363–370, 2002.

[6] A. L. Gray and P. J. Farris-Manning, "Repeat-pass interferometry with airborne synthetic aperture radar," *IEEE Trans. Geosci. Remote Sensing*, vol. 31, pp. 180–191, Jan. 1993.

[7] R. Scheiber, A. Reigber, A. Ulbricht, K. P. Papathanassiou, R. Horn, S. Buckreuß, and A. Moreira, "Overview of interferometric data acquisition and processing modes of the experimental airborne SAR system of DLR," in *Proc. IGARSS*, Hamburg, Germany, 1999, pp. 35–37.

[8] A. Moreira, J. Mittermayer, and R. Scheiber, "Extended chirp scaling algorithm for air- and spaceborne SAR data processing in stripmap and ScanSAR imaging modes," *IEEE Trans. Geosci. Remote Sensing*, vol. 34, pp. 1123–1136, Sept. 1996.

[9] A. Reigber and K. P. Papathanassiou, "Correction of residual motion errors in airborne repeat-pass interferometry," in *Proc. IGARSS*, Sydney, Australia, 2001, pp. 3077–3079.

[10] R. Scheiber and A. Moreira, "Coregistration of interferometric SAR images using spectral diversity," *IEEE Trans. Geosci. Remote Sensing*, vol. 38, pp. 2179–2191, Sept. 2000.

[11] G. Smith and L. M. H. Ulander, "A model relating VHF-band backscatter to forest stem volume," *IEEE Trans. Geosci. Remote Sensing*, vol. 38, pp. 728–740, Mar. 2000.

[12] A. Reigber and J. Moreira, "Phase unwrapping by fusion of local and global methods," in *Proc. IGARSS*, Singapore, 1997, pp. 869–871.

[13] H. A. Zebker, P. A. Rosen, R. M. Goldstein, A. Gabriel, and C. Werner, "On the derivation of coseismic displacement fields using differential radar interferometry: The landers earthquake," *J. Geophys. Res.*, vol. 99, pp. 19 617–19 634, 1994.

[14] D. Alsdorf, L. Smith, and J. Melack, "Amazon floodplain level changes measured with interferometric SIR-C radar," *IEEE Trans. Geosci. Remote Sensing*, vol. 39, pp. 423–431, Feb. 2001.

[15] R. Scheiber and P. Robert, "Origin and correction of phase errors in airborne repeat-pass SAR interferometry," in *Proc. IGARSS*, Sydney, Australia, 2001, pp. 3114–3116.

[16] H. Kimura and N. Ito, "ALOS/PALSAR: The Japanese second-generation spaceborne SAR and its applications," *Proc. SPIE*, vol. 4152, pp. 110–119, 2000.